Electronic Supplementary Information

Directly decorated CeY zeolite for O_2-selective adsorption in O_2/N_2 separation at ambient temperature

Hanbang Liu, [ab] Danhua Yuan, [a] Liping Yang, [ab] Jiacheng Xing, [ab] Shu Zeng, [ab] Shutao Xu, [a] Yunpeng Xu,*[a] and Zhongmin Liu [ab]

a. National Engineering Laboratory for Methanol to Olefins, Dalian National Laboratory for Clean Energy, Dalian Institute of Chemical Physics, Chinese Academy of Sciences, Dalian 116023, P. R. China.

b. University of Chinese Academy of Sciences, Beijing 100049, P. R. China.

* E-mail: xuyunpeng@dicp.ac.cn.

Table of Contents

1 Experimental Section

1.1 Materials

Zeolite NaY (SiO_2/Al_2O_3 = 5.4) were purchased from DALIAN HAIXIN CHEMICAL INDUSTRIAL CO., LTD. 2-methylimidazole (98%), 2-ethylimidazole (≧98%) and 2-propylimidazole (≧95%) were purchased from Aladdin. $Ce(NO_3)_2•6H_2O$ (AR) was purchased from Sinopharm Chemical Reagent Corp. All materials were used without further treatment.

1.2 Preparation of adsorbents

Ion Exchange. 4 g NaY was treated with 200 mL $Ce(NO_3)_2•6H_2O$ solution (0.1 M) at 80 °C under stirring for 4 h and followed by filtration and washing with deionized water 3 times. The above process was repeated 3 times. The obtained sample CeY was dried at 100 ° C for 12 h.

Decoration of imidazole. A suspension solution including 1 g CeY and 10 g deionized water was denoted as **1**. A solution including 3 g 2-methylimidazole (or 3.5 g 2-ethylimidazole, or 4 g 2-propylimidazole) and 30 g deionized water was denoted as **2**. Then, **1** and **2** were mixed together in a beaker and stirred at 60 °C for 4 h. And the samples were thoroughly washed with deionized water to neutral after the reaction was finished. Finally, the samples were dried at 100 °C for 12 h. The obtained samples were denoted as CeY-mIM, CeY-eIM and CeY-pIM respectively. In addition, CeY-pIM-m and CeY-pIM-s samples were obtained by reducing the amount of 2-propylimidazole to 1 g and 0.1 g respectively in the decoration processes.

1.3 Characterizations

The powder X-ray diffraction (**PXRD**) patterns were collected on a PANalytical X'Pert PRO X-ray diffractometer using the Cu-Kα radiation (λ = 1.54059 Å), operating at 40 kV and 40 mA.

Scanning electron microscopy (**SEM**) images were measured on Hitachi SU8020 cold field emission scanning electron microscope.

Inductively Coupled Plasma Optical Emission Spectrometer (**ICP-OES**) analysis were performed on a PerkinElmer 7300DV.

The carbon content of all samples was analyzed by a total organic carbon (**TOC**) analyzer (SSM-5000A; Shimadzu Co.).

Diffuse Reflectance Infrared Fourier Transform Spectroscopy (**DRIFTS**) experiments was carried out on a Bruker Vextex70 spectroscope equipped with an MCT detector. The samples waere placed in the diffuse reflectance infrared chamber with a ZnSe window and heated at 350 °C to remove the adsorbed water. The spectra were detected by collecting 16 scans at resolution of 4 cm^{-1} under flowing N_2.

The ^1H-^{13}C and ^1H-^{15}N cross-polarization/magic-angle spinning solid-state nuclear magnetic (**^{13}C and ^{15}N CP/MAS NMR**) experiments were performed on a Bruker Avance III 600 spectrometer equipped with a 14.1 T wide-bore magnet (the recycle delay is 2 s and the contact time is 3 ms). The resonance frequency for ^{13}C was 150.9 MHz, and for ^{15}N was 60.8 MHz, respectively. A 4 mm WVT probe was used to ^1H-^{13}C CP/MAS with spinning rate of 12 kHz. And a 7 mm HX probe with spinning rate of 5 kHz was used to ^1H-^{15}N CP/MAS. ^{13}C chemical shift was referenced to the upfield methane of adamantane at 29.5 ppm, and ^{15}N chemical shifts was referenced to the glycine at 33.4 ppm.

In situ X-ray photoelectron spectroscopy (**in situ XPS**) was recorded on a EnviroESCA (SPECS) equipped with a differentially pumped energy analyzer connected to an exchangeable sample environment. All samples were in situ heated in vacuum at 300 °C for 1 h before testing. The XPS peaks were calibrated by the binding energy of C 1s peaks at 284.8 eV.

Thermogravimetric analysis (**TGA**) was measured on an SDT Q600 (TA Instruments-Waters LLC, USA) from room temperature to 800 °C in the atmosphere of N_2. And the heat rate was 10 °C /min, the N_2 flow rate was 100 ml/min.

N_2 adsorption-desorption isotherms were measured at -196 ° C by a volumetric adsorption analyzer (Micromeritics, ASAP2020, USA). The specific surface areas (S_{BET}) and total pore volume (V_t) were obtained using the Brunauer-Emmett-Teller (BET) equation. Micropore surface areas (S_{micro}) were calculated based on t-plot method. The pore size distributions were deduced from Density Functional Theory (DFT).

1.4 Gas adsorption and recyclability experiments

Adsorption isotherms of O_2 and N_2 of all samples were measured on a Micromeritics ASAP2050 system at 15, 20 and 25 °C, pressure up to 715 kPa. The O_2 recyclability experiments of CeY-pIM were measured at 25 °C, pressure up to 715 kPa, the desorption step in each cycle was immediately performed on the sample once the adsorption measurement was completed, which was realized by outgassing at 200 °C under high vacuum condition for 2 h. Then, the same procedure was started for

the next adsorption-desorption cycle. In addition, the adsorption-desorption cycle experiments with a lower desorption temperature (100 °C and 25 °C) were also performed. The purity of O_2 and N_2 were 99.999% without any purification.

1.5 Adsorption theories

We used the Langmuir model to fit the single component adsorption isotherms of O_2 and N_2 at 25 °C.[1, 2] The equation can be expressed as follows:

$$q = \frac{q_m bp}{1 + bp}$$

where q is the amounts of O_2 or N_2 adsorbed per mass of adsorbent in equilibrium (mmol/g); q_m is the saturation capacities (mmol/g); b is the adsorption equilibrium constant; p is the total pressure (kPa) of the bulk gas at equilibrium.

The O_2/N_2 selectivity was calculated according to ideal adsorption solution theory (IAST)[3] based on the single component adsorption isotherms of O_2 and N_2. The final adsorption selectivity of O_2 to N_2 was calculated as follows:

$$S_{O_2/N_2} = \frac{x_{O_2}/y_{O_2}}{x_{N_2}/y_{N_2}}$$

where x_{O_2} and x_{N_2} are the mole fractions of O_2 and N_2 in the adsorbed phase; y_{O_2} and y_{N_2} are the mole fractions of O_2 and N_2 in the gas phase.

The isosteric heat of adsorption (Q_{st}) was calculated following Clausius-Clapeyron equation[4, 5]:

$$ln(P) = -\frac{Q_{st}}{RT} + C$$

The single component adsorption isotherms of O_2 and N_2 for CeY and CeY-pIM at 15, 20 and 25 °C were fitted by Langmuir model to obtain the exact pressures that correspond to specific loadings. At each loading, the slope of ln(P) versus 1/T was calculated to obtain the isosteric heat.

1.6 Breakthrough experiments

We used a home-assembled experimental setup to perform the breakthrough experiments.[6, 7] Breakthrough experiments were carried out with binary mixtures of O_2/N_2 (21/79, v/v) at 25 °C for feed gas at 100 kPa flowing at 10 mL/min. Before the experiments, a stainless adsorption column (diameter: 8 mm, length: 30 cm) were filled with adsorbent sample pellets. The adsorbent was activated in situ by flowing pure He (60 mL/min) through the column and raising the temperature to 250 °C with a residence time of 4 h before the measurements. And this process was also used to carry out the regeneration of adsorbents. We used I/I_0 as the ordinate to normalize the breakthrough results, I_0 is the intensity after N_2 or O_2 reaches adsorption equilibrium measured by mass spectrometry.

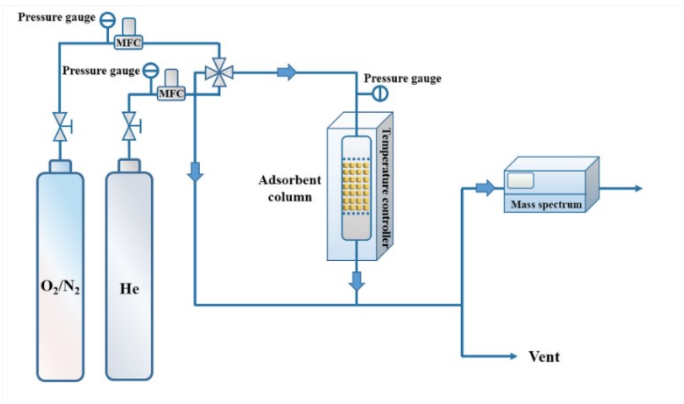

Fig. S1 The breakthrough experiment setup. MFC: mass flow controller.

1.7 Molecular Simulation Details

Molecular simulation was carried out by Materials Studio, using the CASTEP module. The Perdew-Burke-Ernzerh (PBE) exchange-correlation functional within the generalized gradient approach (GGA) was used to perform Density functional theory (DFT) calculations.[8, 9] To converge the total energy and electron density difference, a self consistent field (SCF) tolerance of 0.1 meV/atom, a cutoff energy of 600 eV and a 1×1×1 k-point mesh were installed. The simplified Ce/Si-O-Al and Ce-pIM/Si-O-Al clusters were used to replace the complex structures of CeY and CeY-pIM, respectively.[6, 10] All structure were optimized before introducing O_2 and N_2 molecules to Ce/Si-O-Al and Ce-pIM/Si-O-Al models. After introducing the guest molecule and optimizing structure, the electron density difference of O_2 and N_2 in above clusters were analyzed. In addition, the Ce-N distances of Ce-pIM/Si-O-Al cluster under different conditions were calculated. The single-point energy of optimized O_2 and N_2 were calculated by placing them in a cell which had the same cell dimensions as the cluster models respectively. Interaction energies (IE) between the cluster and O_2/N_2 molecules and the difference (ΔE) between them were calculated as:

$$IE\text{-}N_2 = E(cluster + N_2) - E(cluster) - E(N_2)$$

$$IE\text{-}O_2 = E(cluster + O_2) - E(cluster) - E(O_2)$$

$$\Delta E = (IE\text{-}O_2) - (IE\text{-}N_2)$$

where E(cluster + O_2) and E(cluster + N_2) are the total energies of the optimized cluster-O_2 and cluster-N_2 complex, E(cluster), E(O_2) and E(N_2) are the single-point energies of cluster, O_2 and N_2, respectively.

2 Results and Discussion

2.1 Supplementary Figures

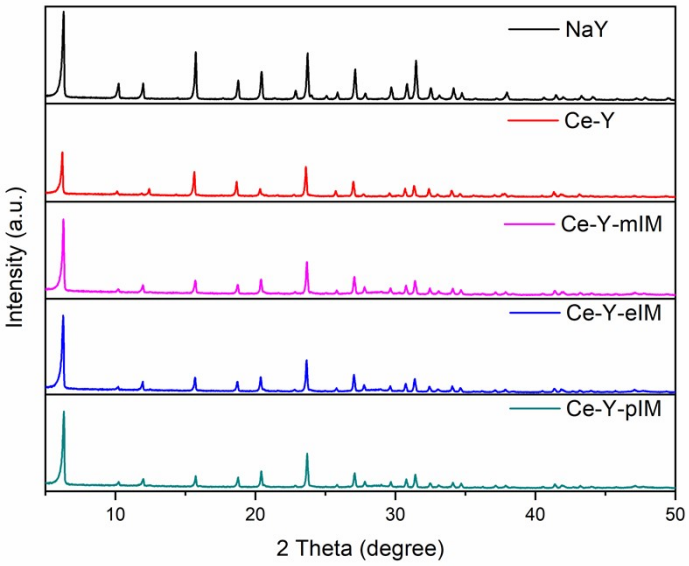

Fig. S2 PXRD patterns of NaY, CeY, CeY-mIM, CeY-eIM and CeY-pIM.

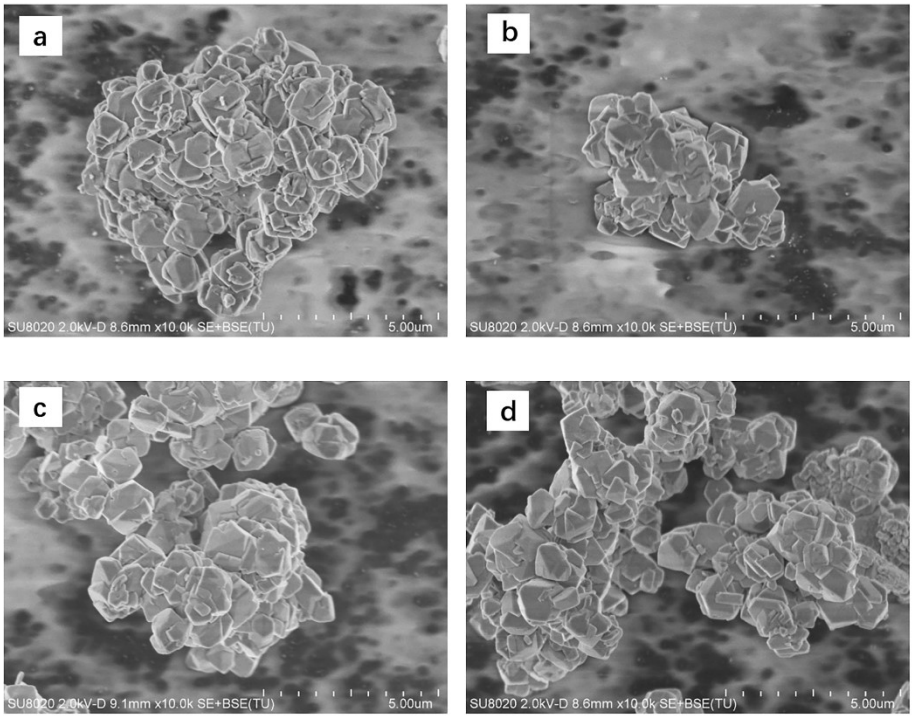

Fig. S3 SEM images of (a) CeY, (b) CeY-mIM, (c) CeY-eIm and (d) CeY-pIM.

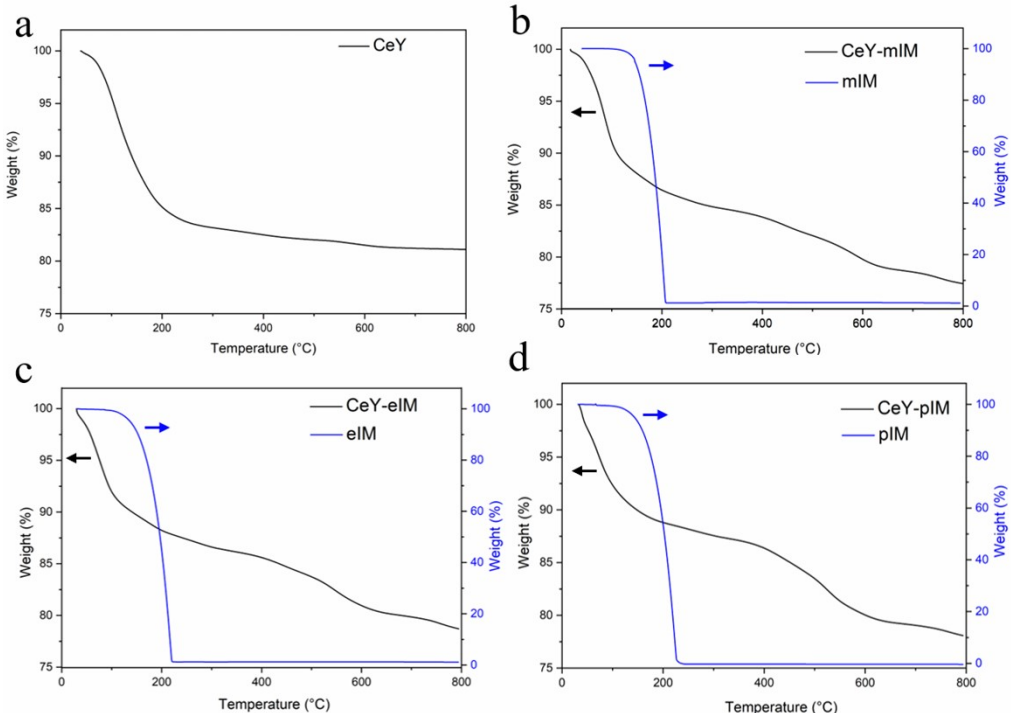

Fig. S4 TG curves of all samples and pure imidazole chemicals.

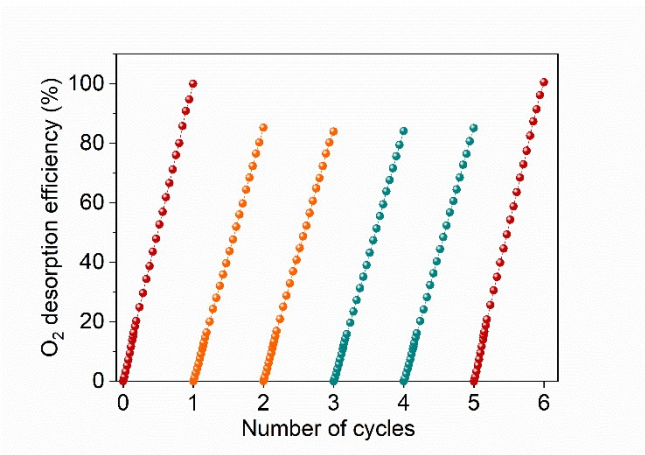

Fig. S5 Cyclic regeneration experiments for O_2 adsorption on CeY-pIM at 25 °C and pressures up to 715 kPa. For cycle 1 and 2 (orange), the desorption temperature is 100 °C before adsorbing; for cycle 3 and 4 (cyan), the desorption temperature is 25 °C before adsorbing; for cycle 0 and the last cycle (red), the desorption temperature before adsorbing is 200 °C.

The adsorption-desorption cycle experiments of the CeY-pIM with low desorption temperature (100 °C and 25°C) were performed. As shown in Fig. S5, CeY-pIM displayed a loss (about 15 %) in capacity after desorption with 100 °C, which is due to the strong interaction between modified Ce sites and O_2. In addition, almost no capacity loss occurred in the subsequent adsorption-desorption cycles by using a lower desorption temperature (25 °C), indicating that the adsorption performance of CeY-pIM can be well maintained even at a relatively low desorption temperature. And after increasing the desorption temperature to 200 °C, the O_2 uptake on CeY-pIM returned to the original level as shown in the last cycle.

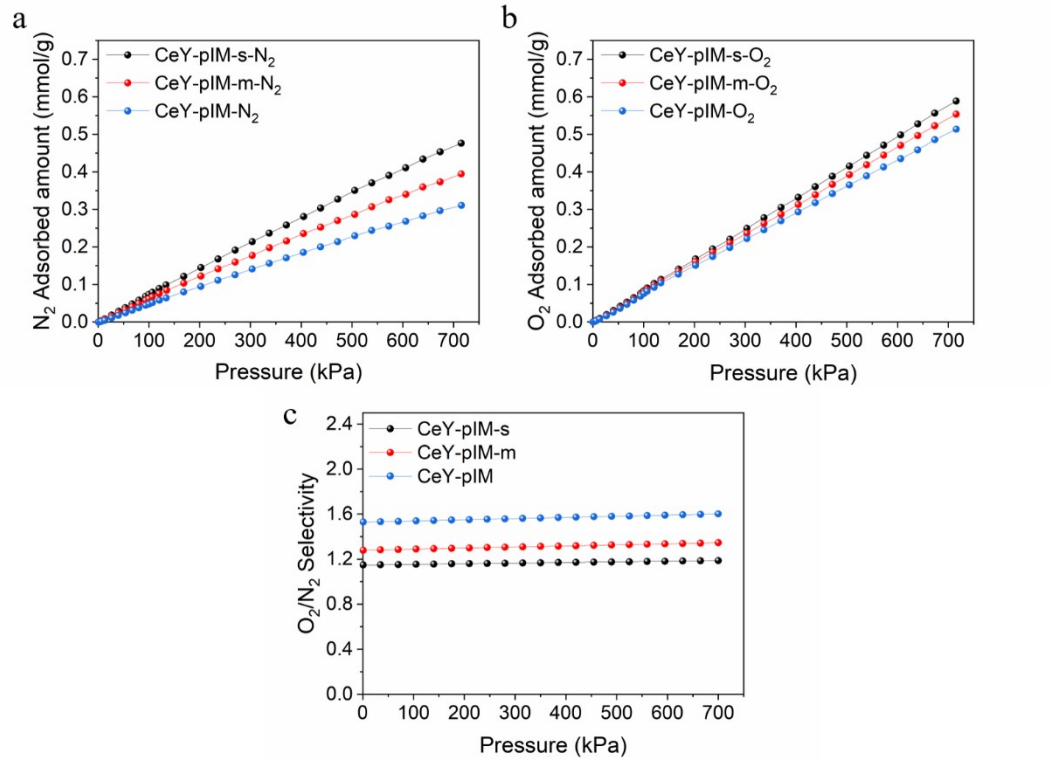

Fig. S6 The single-component (a) N_2 and (b) O_2 adsorption isotherms of all pIM-modified samples at 25 °C. (c) IAST-predicted selectivities for O_2/N_2 mixtures (21:79) on all pIM-modified samples at 25 °C.

CeY-pIM-m and CeY-pIM-s samples were obtained by reducing the amount of imidazole during the preparation processes, and their imidazole content is less than that of CeY-pIM as shown in Table S1. As shown in Fig. S6, the N_2 and O_2 uptakes on CeY-pIM-s at 715 kPa were 0.477 mmol/g and 0.589 mmol/g, respectively, which were higher than that of CeY-pIM-m (0.395 mmol/g for N_2 uptake, 0.554 mmol/g for O_2 uptake), and CeY-pIM had the lowest N_2 and O_2 uptakes (0.311 mmol/g for N_2 uptake, 0.514 mmol/g for O_2 uptake). However, it is worth noting that the O_2/N_2 selectivity order for them is CeY-pIM-s < CeY-pIM-m < CeY-pIM as shown in Fig. S6c. The increase of imidazole molecules occupying the pores of zeolites can make zeolite absorb less O_2 and N_2, which is consistent with the experimental results. In addition, the electric field of zeolite framework will be weakened as the increase of imidazole, thereby weakening the interaction with N_2 that has high quadrupole moment, results in an additional reduction of N_2 uptake. In conclusion, the content of imidazole has an opposite effect on the O_2 adsorption capacity and selectivity of modified samples: high imidazole content will reduce their O_2 and N_2 uptakes, but their O_2/N_2 selectivities will increase.

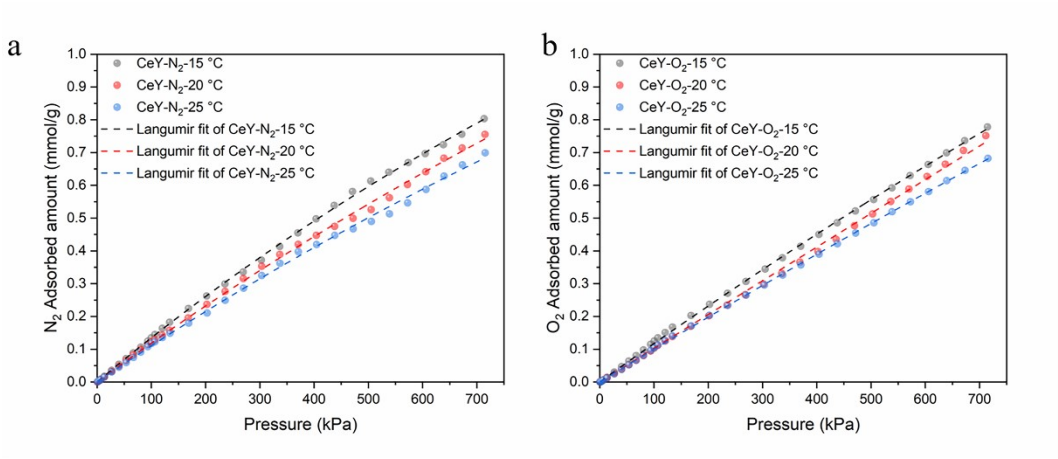

Fig. S7 Adsorption isotherms and Langmuir fitting curves of N_2 (a) and O_2 (b) on CeY at 15, 20 and 25 °C.

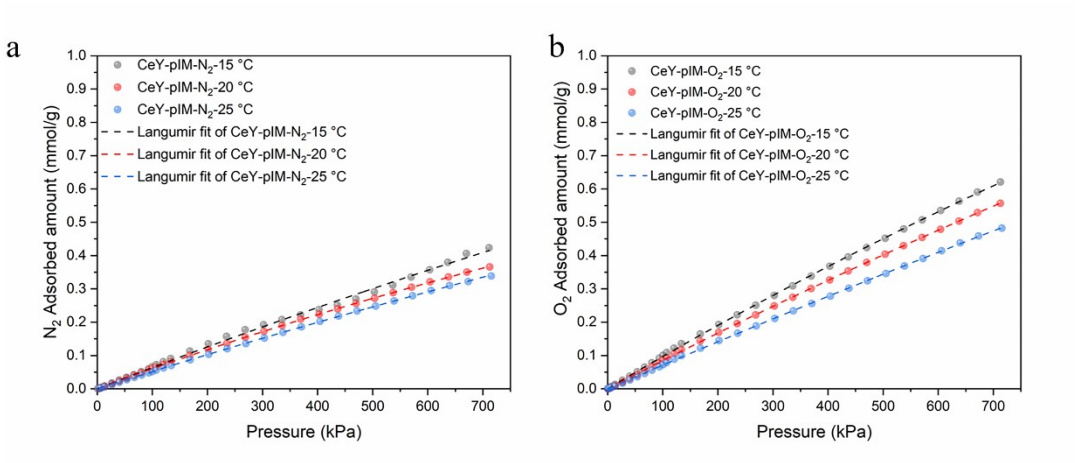

Fig. S8 Adsorption isotherms and Langmuir fitting curves of N_2 (a) and O_2 (b) on CeY-pIM at 15, 20 and 25 °C.

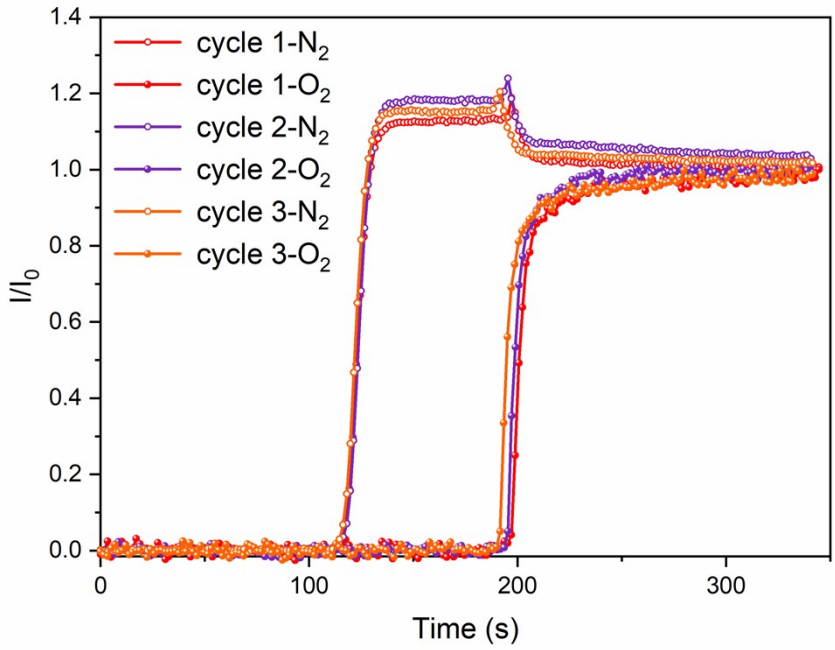

Fig. S9 Breakthrough cycle experiments of O_2/N_2 (21:79, v/v) on CeY-pIM at 100 kPa and 25 °C.

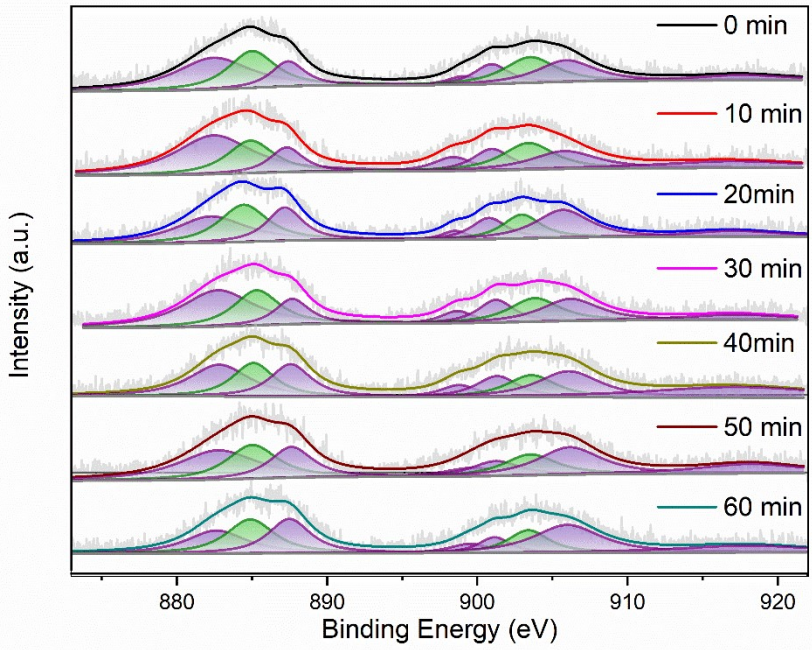

Fig. S10 In situ Ce 3d XPS spectra of CeY in N_2 atmosphere at 25 °C.

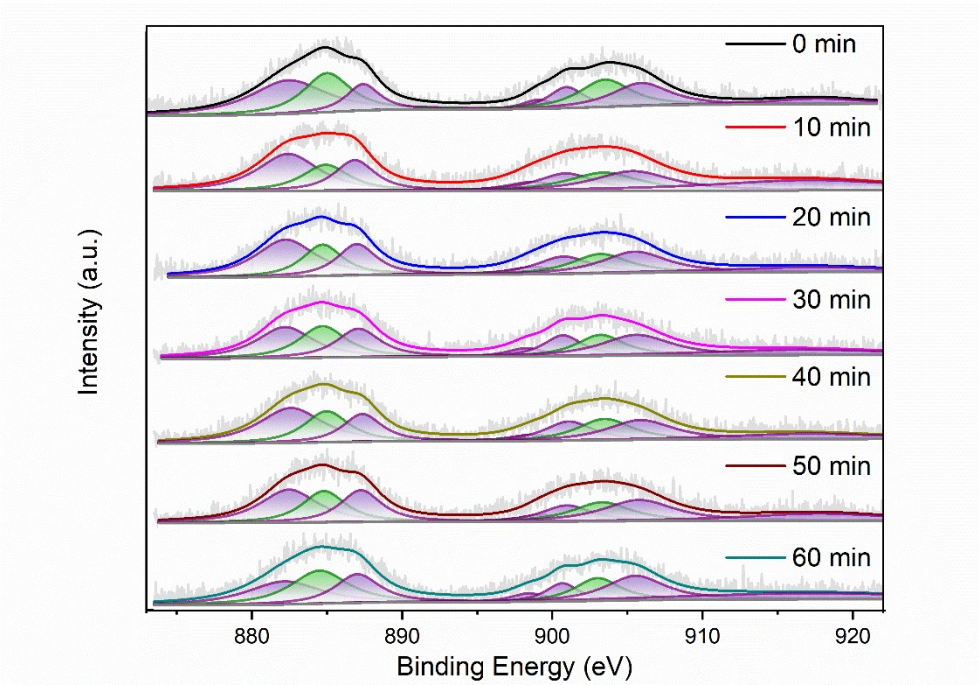

Fig. S11 In situ Ce 3d XPS spectra of CeY in O_2 atmosphere at 25 °C.

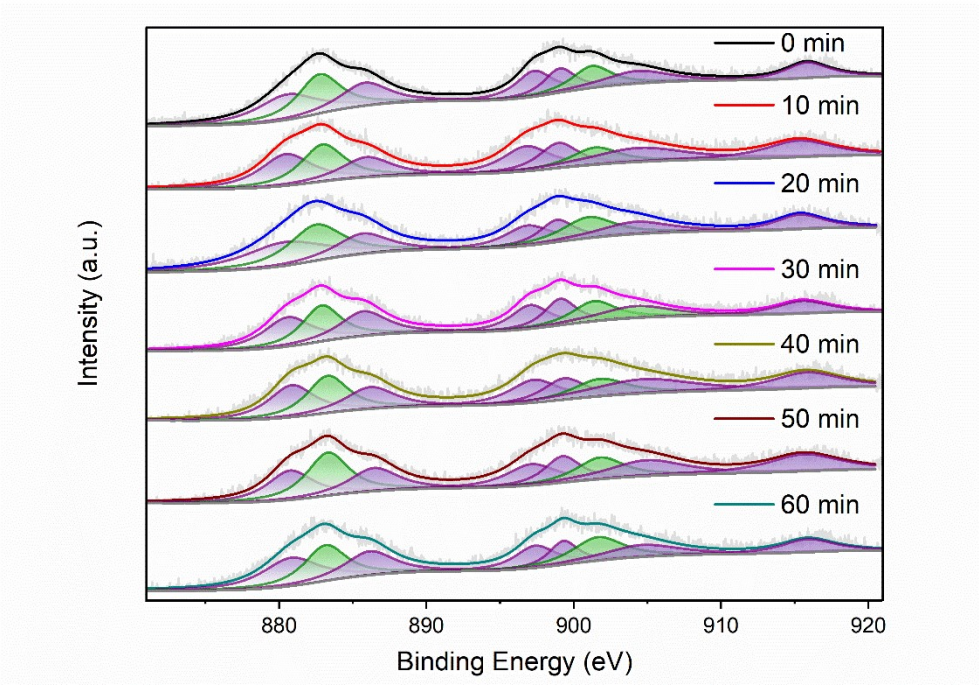

Fig. S12 In situ Ce 3d XPS spectra of CeY-pIM in N_2 atmosphere at 25 °C.

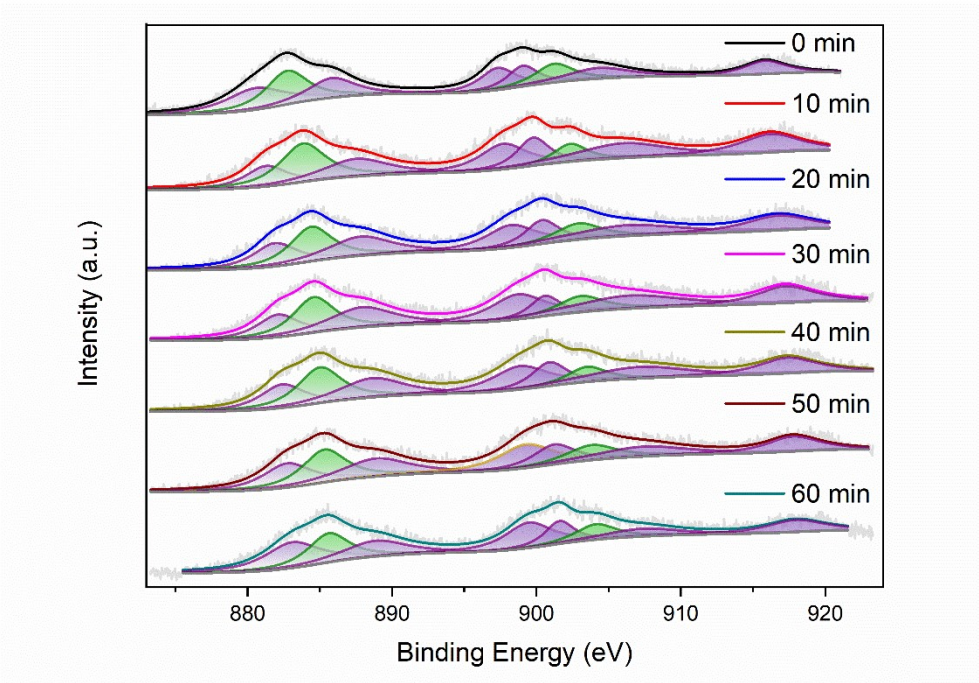

Fig. S13 In situ Ce 3d XPS spectra of CeY-pIM in O_2 atmosphere at 25 °C.

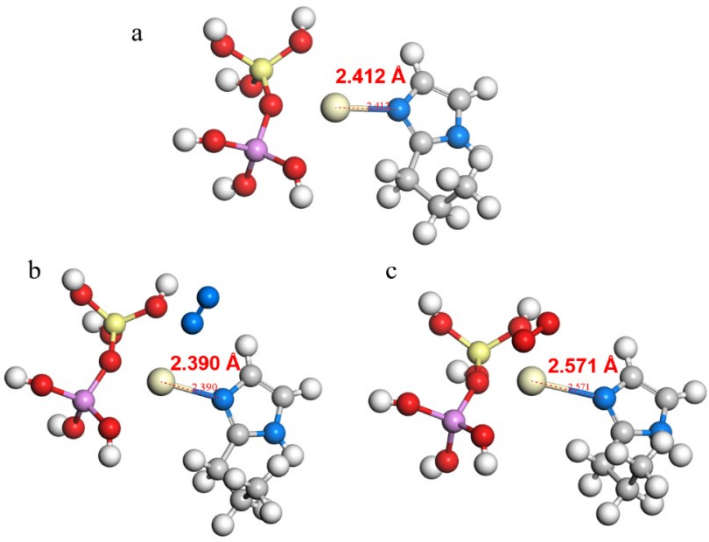

Fig. S14 (a) The Ce-N distance of Ce-pIM/Si-O-Al cluster under vacuum in simulations. (b) The Ce-N distance of Ce-pIM/Si-O-Al cluster after adsorbing N_2 in simulations. (c) The Ce-N distance of Ce-pIM/Si-O-Al cluster after adsorbing O_2 in simulations. Ce: light yellow, O: red, N: light blue, Si: yellow, Al: violet, C: brown, H: white.

The Ce-N distance of Ce-pIM/Si-O-Al cluster under vacuum is about 2.412 Å, which is similar to some Ce-MOFs[11, 12], and it also indicates that Ce ion of zeolite actually combines with the N atom of imidazole. In addition, the change of their Ce-N distances after adsorbing N_2 and O_2 is worth noting. After introducing N_2, the Ce-N distance of Ce-pIM/Si-O-Al cluster has almost no change. However, its Ce-N distance elongates significantly after introducing O_2. This result shows that the Ce sites of modified sample have relatively strong electron transfer interaction with O_2, which weakens the combination of Ce and N atom of imidazole and increases the Ce-N distance.

2.2 Supplementary Tables

Table S1. ICP-OES and TOC results of all samples.

Sample	Ce wt%[a]	C wt%[b]	IM/Ce molar ratio
CeY	10.31	0.31	-
CeY-mIM	10.46	5.7	1.6
CeY-eIM	11.02	6.7	1.4
CeY-pIM	10.73	8.3	1.5
CeY-pIM-m	12.70	6.9	1.1
CeY-pIM-s	12.16	5.4	0.9

[a] Ce content was measured by ICP-OES. [b] C content was measured by TOC analyzer. [c] IM/Ce molar ratios were calculated based on the results of Ce and C content.

Table S2. Fitting parameters of the Langmuir adsorption model used to calculate IAST selectivity.

Parameters	adsorbate	q_m	b	R^2
CeY	O_2	21.831	0.0000433	0.999832
	N_2	5.299	0.000214	0.999565
CeY-mIM	O_2	11.618	0.0000881	0.999957
	N_2	4.0784	0.000201	0.999737
CeY-eIM	O_2	8.566	0.000109	0.999936
	N_2	3.743	0.000185	0.999885
CeY-pIM	O_2	12.473	0.0000598	0.999917
	N_2	3.103	0.000162	0.999717
CeY-pIM-m	O_2	15.671	0.0000509	0.999933
	N_2	3.439	0.000181	0.999704
CeY-pIM-s	O_2	14.926	0.0000568	0.999938
	N_2	5.070	0.000146	0.999837

Table S3. Comparison of O_2 and N_2 uptakes at 100 kPa and O_2/N_2 selectivity between CeY-pIM and some MOFs/zeolite adsorbents.

Adsorbent	Temperature (°C)	O_2 uptake (mmol/g)	N_2 uptake (mmol/g)	O_2/N_2 Selectivity	O_2/N_2 (v:v)	reference
Fe_2(dobdc)	-72 °C	9.5	6.9	11[a]	21/79	13
Co-BTTri	-78 °C	4.8	2.0	41[a]	21/79	14
Fe-BTTri	-78 °C	5.9	4.0	27[a]	21/79	15
$Co_2(OH)_2$(BBTA)	25 °C	1.09	0.20	49[a]	21/79	16
$Cu(Qc)_2$	25 °C	0.079	0.027	3.33[a]	21/78	17
$Cr_3(btc)_2$	25 °C	3.43	0.21	22[b]	21/78	18
Cr-BTT	25 °C	2.37	0.25	2570[a]	20/80	19
Sc-MIL-100	25 °C	0.26	0.19	1.25[a]	20/80	20
Fe-MIL-100	25 °C	0.24	0.18	1.25[a]	20/80	20
MOF-177	25 °C	0.18	0.1	1.8[b]	50/50	21
Na-Ce type X	22 °C	0.17	0.18	1.79[c]	50/50	22
NaUZM-9-H	25 °C	0.20	0.15	1.3[a]	21/79	23
CeY-pIM	25 °C	0.076	0.048	1.6[a]	21/79	This work

[a] The selectivity was calculated by ideal adsorbed solution theory (IAST). [b] The selectivity was calculated by uptake ratio. [c] The selectivity was calculated by Henry's constant.

3 References

1. B. Li, Y. Zhang, R. Krishna, K. Yao, Y. Han, Z. Wu, D. Ma, Z. Shi, T. Pham, B. Space, J. Liu, P. K. Thallapally, J. Liu, M. Chrzanowski and S. Ma, *J. Am. Chem. Soc.*, 2014, **136**, 8654-8660.
2. A. Pal, S. Chand, D. G. Madden, D. Franz, L. Ritter, A. Johnson, B. Space, T. Curtin and M. C. Das, *Inorg. Chem.*, 2019, **58**, 11553-11560.
3. A. L. Myers and J. M. Prausnitz, *AIChE J.*, 1965, **11**, 121-127.
4. Y. Zhang, H. Xiao, X. Zhou, X. Wang and Z. Li, *Ind. Eng. Chem. Res.*, 2017, **56**, 8689-8696.
5. D. Lv, R. Shi, Y. Chen, Y. Wu, H. Wu, H. Xi, Q. Xia and Z. Li, *ACS Appl. Mater. Interfaces*, 2018, **10**, 8366-8373.
6. Y. Q. Wu, D. H. Yuan, D. W. He, J. C. Xing, S. Zeng, S. T. Xu, Y. P. Xu and Z. M. Liu, *Angew. Chem. Int. Ed.*, 2019, **58**, 10241-10244.
7. Y. Wu, S. Zeng, D. Yuan, J. Xing, H. Liu, S. Xu, Y. Wei, Y. Xu and Z. Liu, *Angew. Chem. Int. Ed.*, 2020, **59**, 6765-6768.
8. M. H. Rosnes, D. Sheptyakov, A. Franz, M. Frontzek, P. D. C. Dietzel and P. A. Georgiev, *Phys. Chem. Chem. Phys.*, 2017, **19**, 26346-26357.
9. X. Cui, K. Chen, H. Xing, Q. Yang, R. Krishna, Z. Bao, H. Wu, W. Zhou, X. Dong, Y. Han, B. Li, Q.

Ren, M. J. Zaworotko and B. Chen, *Science*, 2016, **353**, 141-144.

10. Y. Kuwahara, K. Nishizawa, T. Nakajima, T. Kamegawa, K. Mori and H. Yamashita, *J. Am. Chem. Soc.*, 2011, **133**, 12462-12465.
11. J. Ethiraj, F. Bonino, J. G. Vitillo, K. A. Lomachenko, C. Lamberti, H. Reinsch, K. P. Lillerud and S. Bordiga, *Chemsuschem*, 2016, **9**, 713-719.
12. O. Ayhan, I. L. Malaestean, A. Ellern, J. van Leusen, S. G. Baca and P. Koegerler, *Cryst. Growth Des.*, 2014, **14**, 3541-3548.
13. E. D. Bloch, L. J. Murray, W. L. Queen, S. Chavan, S. N. Maximoff, J. P. Bigi, R. Krishna, V. K. Peterson, F. Grandjean, G. J. Long, B. Smit, S. Bordiga, C. M. Brown and J. R. Long, *J. Am. Chem. Soc.*, 2011, **133**, 14814-14822.
14. D. J. Xiao, M. I. Gonzalez, L. E. Darago, K. D. Vogiatzis, E. Haldoupis, L. Gagliardi and J. R. Long, *J. Am. Chem. Soc.*, 2016, **138**, 7161-7170.
15. D. A. Reed, D. J. Xiao, H. Z. H. Jiang, K. Chakarawet, J. Oktawiec and J. R. Long, *Chem. Sci.*, 2020, **11**, 1698-1702.
16. A. S. Rosen, M. R. Mian, T. Islamoglu, H. Chen, O. K. Farha, J. M. Notestein and R. Q. Snurr, *J. Am. Chem. Soc.*, 2020, **142**, 4317-4328.
17. Y. Tang, X. Wang, Y. Wen, X. Zhou and Z. Li, *Ind. Eng. Chem. Res.*, 2020, **59**, 6219-6225.
18. L. J. Murray, M. Dinca, J. Yano, S. Chavan, S. Bordiga, C. M. Brown and J. R. Long, *J. Am. Chem. Soc.*, 2010, **132**, 7856-7857.
19. E. D. Bloch, W. L. Queen, M. R. Hudson, J. A. Mason, D. J. Xiao, L. J. Murray, R. Flacau, C. M. Brown and J. R. Long, *Angew. Chem. Int. Ed.*, 2016, **55**, 8605-8609.
20. D. F. Sava Gallis, K. W. Chapman, M. A. Rodriguez, J. A. Greathouse, M. V. Parkes and T. M. Nenoff, *Chem. Mater.*, 2016, **28**, 3327-3336.
21. Y. Li and R. T. Yang, *Langmuir*, 2007, **23**, 12937-12944.
22. A. Jayaraman, R. T. Yang, S. H. Cho, T. S. G. Bhat and V. N. Choudary, *Adsorption*, 2002, **8**, 271-278.
23. H. Liu, D. Yuan, G. Liu, J. Xing, Z. Liu and Y. Xu, *Chem. Commun.*, 2020, **56**, 11130-11133.